



# CHORUS

This is the accepted manuscript made available via CHORUS. The article has been published as:

## Transport Theory of Monolayer Transition-Metal Dichalcogenides through Symmetry

Yang Song and Hanan Dery

Phys. Rev. Lett. **111**, 026601 — Published 9 July 2013

DOI: [10.1103/PhysRevLett.111.026601](https://doi.org/10.1103/PhysRevLett.111.026601)

# Transport Theory of Monolayer Transition-Metal Dichalcogenides through Symmetry

Yang Song<sup>1,\*</sup> and Hanan Dery<sup>2,1</sup>

<sup>1</sup>*Department of Physics and Astronomy, University of Rochester, Rochester, New York, 14627*

<sup>2</sup>*Department of Electrical and Computer Engineering,  
University of Rochester, Rochester, New York, 14627*

We present a theory that elucidates the major momentum and spin relaxation processes for electrons, holes and hot excitons in monolayer transition-metal dichalcogenides. We expand on spin flips induced by flexural phonons and show that the spin relaxation is ultrafast for electrons in free-standing membranes while being mitigated in supported membranes. This behavior due to interaction with flexural phonons is universal in 2D membranes that respect mirror symmetry and it leads to a counterintuitive inverse relation between mobility and spin relaxation.

PACS numbers:

Single-layer transition-metal dichalcogenides (SL-TMDs) put together exotic charge, spin and valley electronic phenomena in a simple 2D solid-state system [1–3]. Recent advances in characterization of these materials have sparked a wide interest in their *d*-band semiconducting behavior and spin-valley coupling [4–7]. Room-temperature mobility of the order of  $100 \text{ cm}^2/\text{V}\cdot\text{s}$  in *n*-type MoS<sub>2</sub> monolayer transistor was demonstrated and analyzed [8–10]. In addition, the unique time-reversal relations between spin and valley degrees of freedom were studied from the exciton photoluminescence (PL) [11–14]. In spite of these recent advances and supporting studies of band-structure and phonons parameters [15–20], there is still no unifying description of the spin and charge transport in these materials.

In this Letter, we present a theory that elucidates the intrinsic momentum and spin relaxation mechanisms in SL-TMDs. We first delineate the transport limitations at elevated temperatures via zeroth-order selection rules and make connection with the energy relaxation of hot excitons. It is shown that spin-conserving scattering between direct and indirect exciton bands leads to reduction in the circular polarization degree of the PL. Then, we analyze the intriguing physics of spin relaxation due to scattering with long-wavelength flexural phonons and compare the findings with the case of graphene. Ultrafast spin relaxation of electrons is predicted for free-standing SL-TMDs whereas for supported membranes the spin lifetime is greatly enhanced. Finally, we discuss the relation between spin relaxation and charge mobility.

Figure 1(a) shows the trigonal prismatic lattice structure of monolayer MX<sub>2</sub> where M (X) denotes the transition-metal (chalcogen) atom. The lack of space-inversion center lowers the symmetry compared with monolayer graphene, leading to spin-split energy bands as shown in Fig. 1(b). Rather than invoking elaborate numerical techniques, we explain the essential transport properties of SL-TMDs by rendering the transformation properties of pertinent electronic states and atomic displacements. This information is captured by the irreducible representations (IRs), shown in Fig. 1(b) for edge

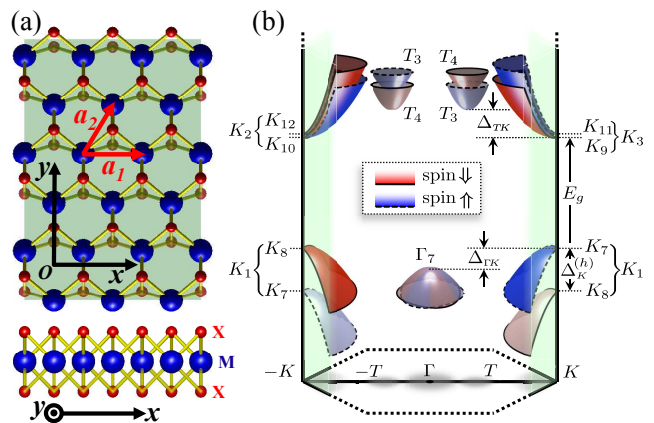


FIG. 1: (Color online) (a) Top and side views of the real space lattice. (b) Typical scheme of primary and satellite valleys in the conduction and valence bands.

states of the conduction and valence bands [21]. We begin with the electron-phonon interaction in its zeroth order, characterized by nonvanishing scattering amplitude between band-edge states [22]. In experiments, these processes are identified by their temperature dependence (Bose-Einstein distribution of the involved phonon). Table I lists the selection rules, and Fig. 2 shows the underlying atomic displacements for cases of zone-center phonons. With the exception of  $\Gamma_4$  that corresponds to zeroth-order spin flips in the T valleys, energies of all other phonon modes are non-negligible [21]. Thus, only at elevated temperatures the transport in the *K* valleys is affected by zeroth-order processes.

We summarize the physics encompassed in Table I. The intravalley relaxation of either electrons or holes is induced by homopolar scattering due to an out-of-phase displacement of the two chalcogen atomic layers. As implied from Fig. 2(a) and (b) for the respective cases of momentum and spin relaxation, the relaxation is governed by short-range scattering (i.e., the effective charge dipole from these long-wavelength displacements is zero). The intravalley momentum relaxation is caused by thick-

TABLE I: Zeroth-order selection rules in  $\text{MX}_2$  compounds. For spin-conserving scattering, double-group IRs are replaced with simpler single-group IRs. Time reversal symmetry connects  $K$  and  $-K$  points (e.g.,  $K_9=K_{10}^*$  and  $K_2=K_3^*$ ).

Valleys	spin-conserving	spin-flip
Intra	$(X \times X^*)^* = \Gamma_1$ $X = \{K_{1-3}, T_1, \Gamma_1\}$	$(K_{11} \times K_9^*)^* = \Gamma_5$ $(T_3 \times T_4^*)^* = \Gamma_4$
Inter	$(K_3 \times K_2^*)^* = K_3$ $(K_1 \times K_1^*)^* = K_1$ $(T_1 \times K_3^*)^* = T_1$ $(\Gamma_1 \times K_1^*)^* = K_1$	$(T_3 \times K_9^*)^* = T_2$ $(\Gamma_{7\downarrow} \times K_7^*)^* = K_6$

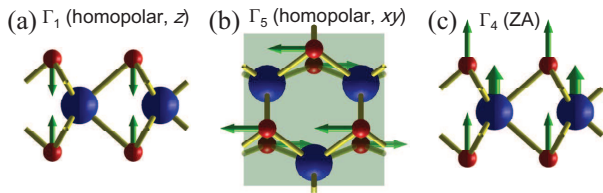


FIG. 2: (Color online) Atomic displacements of the  $\Gamma$  phonon modes involved in zeroth-order scattering.

ness fluctuations of the layer due to the out-of-plane motion of the chalcogen atoms [Fig. 2(a)]. This physical picture was first identified by Fivaz and Mooser [15], and supported by *ab initio* calculations of Kaasbjerg *et al*'s who also showed a comparable contribution to the charge mobility from Fröhlich interaction [10]. Zeroth-order spin flips in the  $K$  valleys are enabled uniquely by homopolar in-plane optical phonons which do not exist in graphene structures [Fig. 2(b)].

The intervalley scattering between primary and satellite valleys ( $K \times T$  &  $K \times \Gamma$ ) is relevant due to the flat nature of the  $d$  bands in SL-TMDs. This scattering is likely to facilitate the Gunn effect when applying a large in-plane electric field [23]. Namely, accelerated carriers are scattered to the satellite valleys in which the mobility and spin relaxation rates are different [24, 25].  $\text{MX}_2$  compounds with heavy (light) chalcogen atoms have a relatively small  $\Delta_{TK}$  ( $\Delta_{\Gamma K}$ ) energy spacing [18], and therefore can be used as  $n$ -type ( $p$ -type) Gunn diodes. Finally, we discuss the nonvanishing intervalley scattering between edges of the  $K$  and  $-K$  valleys. The selection rules show that such scattering largely affects the charge but not the spin transport. The lowest-order spin-flip of either electrons or holes is forbidden by time reversal symmetry. The conduction-band rule ( $K_3 \times K_2^*$ ) is relevant for electron transport in  $n$ -type monolayers [10]. The valence-band rule ( $K_1 \times K_1^*$ ), however, is likely to affect less the transport of holes due to the relatively large energy splitting ( $K_8 \leftrightarrow K_8$  or  $K_7 \leftrightarrow K_7$  intervalley transitions in Fig. 1).

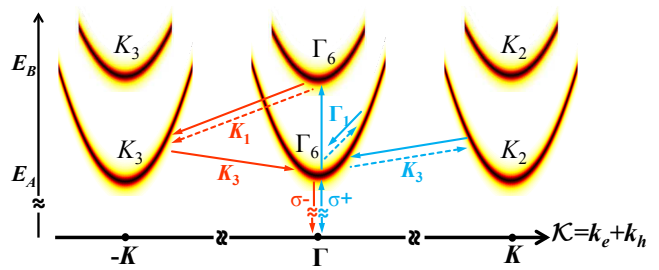


FIG. 3: (Color online) Direct and indirect exciton bands. The optical and exciton-phonon scattering processes are sketched under  $\sigma_+$  photon excitation. Real (virtual) scattering is denoted by solid (dashed) lines and phonon IRs are marked. Right blue (left red) paths lead to  $\sigma_+$  ( $\sigma_-$ ) luminescence.

As an important application, we show that spin-conserving scattering between  $K$  and  $-K$  valleys is imperative for understanding recent exciton PL measurements [11–14]. Figure 3 shows the exciton bands of singlet composites (‘bright excitons’), where upper and lower branches are due to the valence-band spin splitting [26]. The zone-center bands comprise electron and hole states of the same  $K$  valley (direct excitons), where each of the doubly-degenerate zone-center states transform as  $\Gamma_6$  and include  $m_l = \pm 1$  excitons depending on light helicity. Zone-edge bands, on the other hand, belong to  $K_{2,3}$  and comprise electrons and holes from opposite  $K$  valleys (indirect excitons). In the supplemental material we quantify the circular polarization degree of the PL by modeling the absorption and relaxation processes that precede recombination. Here, we summarize this physics and show the relation with selection rules. First, when the exciting photon energy is between  $E_A$  and  $E_B$  (Fig. 3), both upper and lower bands are excited due to energy broadening by impurities and substrate imperfections [11, 12, 14]. Second, the phonon-assisted indirect absorption, a second-order process shown by dashed arrows in Fig. 3, cannot be neglected since it has many more available final states compared with the direct absorption that is limited to  $\mathcal{K} = \mathbf{k}_e + \mathbf{k}_h = 0$  [27]. Third, the intervalley scattering during the relaxation from the upper to lower  $\Gamma_6$  band flips  $m_l$  without a spin-flip of the electron or hole [28]. The missing angular momentum is carried by  $K_1$  and  $K_3$  phonons, as implied from Table I and visualized in Fig. 3 for  $\sigma_+$  excitation. This rapid relaxation explains the measured reduction in the circular polarization degree [14], and it is enabled in multivalley direct-gap SL-TMDs due to the (so-far ignored) unique coexistence of direct and indirect exciton bands.

In the remainder of the Letter, we study the transport due to interaction with long-wavelength acoustic phonons. As in other materials, the vanishing energies of these phonons render this nonzero-order interaction important. We first mention the fundamental distinction between charge and spin transport in monolay-

ers that respect mirror symmetry (e.g., graphene and SL-TMDs). For interactions with single phonons, spin-conserving scattering is not affected by long-wavelength flexures in the out-of-plane direction [29], whereas spin-flip scattering induced by flexural phonon does not vanish [the ZA mode in Fig. 2(c)]. Mathematically, it is understood from the scattering integral,  $\langle \mathbf{s}_f | \nabla \mathcal{V} | \mathbf{s}_i \rangle$ , where in-plane  $\partial \mathcal{V} / \partial r_{\parallel}$  (out-of-plane  $\partial \mathcal{V} / \partial z$ ) deformations are even (odd) with respect to mirror symmetry which also brings in  $\pm 1$  for  $\mathbf{s}_i = \pm \mathbf{s}_f$ .

We focus on the Elliott-Yafet spin-flip mechanism due to the intrinsic electron-phonon scattering [30, 31]. Using the method of invariants [32], the spin-flip transition amplitudes from scattering with flexural phonons are compactly expressed as

$$\mathcal{T}_{ZA,\mathbf{q}}^{sf} \approx \sqrt{\frac{k_B T}{2 \varrho A \gamma^2 q^{2\eta}}} g(\mathbf{k}_i, \mathbf{k}_f), \quad (1)$$

where  $\varrho$  is the areal mass density and  $A$  is the area.  $\gamma$  and  $\eta$  are mechanically-dependent parameters that set the flexural-phonon dispersion. Their values will be introduced when estimating the spin lifetimes in different monolayer conditions.  $\mathbf{q} = \mathbf{k}_i - \mathbf{k}_f$  denotes the small phonon wavevector where  $\mathbf{k}_i$  and  $\mathbf{k}_f$  are wavevectors of the initial and final electronic state, respectively.  $g(\mathbf{k}_i, \mathbf{k}_f)$  depends on the valley position and reads  $\Xi_{\Gamma_1}^{so} |\mathbf{k}_i + \mathbf{k}_f| q$  in the zone-center,  $\Xi_K^{so} q$  in the zone-edge, or  $\Xi_{T_1}^{so}$  in-between.  $\Xi_X^{so}$  are spin-orbit coupling scattering constants [21]. The linear wavevector dependence of  $g(\mathbf{k}_i, \mathbf{k}_f)$  in the zone edge enables estimation of  $\Xi_K^{so}$  from the energy change of the  $K$ -point spin splitting in response to static strain. By symmetry, shear-strain components of the form  $\epsilon_{\pm} = \epsilon_{xz} \pm i\epsilon_{yz}$  are associated with frozen flexural phonons. By focusing on the spin dependent part of the static strain Hamiltonian at  $\mathbf{k} = \mathbf{K}$ ,

$$H_0 + H^{so}(\epsilon_{\pm}) = \begin{pmatrix} b|\epsilon_{+}|^2 & a\epsilon_{+} \\ a\epsilon_{-} & \Delta_K - b|\epsilon_{+}|^2 \end{pmatrix}, \quad (2)$$

we find that  $a = \Xi_K^{so}$  [21].  $a$  and  $b$  are spin-dependent shear deformation potentials, and  $\Delta_K$  is the spin splitting without strain. The value of  $\Xi_K^{so}$ , needed for estimation of the spin relaxation, can now be readily extracted from the strain-induced spin splitting  $\sqrt{(\Delta_K + 2b|\epsilon_{+}|^2)^2 + |2a\epsilon_{+}|^2}$ . Using ABINIT (an open-source DFT code) with Hartwigsen-Goedecker-Hutter pseudopotentials, we find that  $\Xi_K^{so}$  for monolayer MoS<sub>2</sub>, MoSe<sub>2</sub>, WS<sub>2</sub> and WSe<sub>2</sub> are respectively 0.2, 0.27, 0.66 and 0.67 eV in the conduction band [21, 33], and similar magnitudes in the valence band. A notable feature in the conduction band of SL-TMDs is that  $\Delta_K$  can be much smaller than  $\Xi_K^{so}$ : whereas  $\Delta_K$  is mostly governed by the small deviation of the state from centrosymmetric  $d_{z^2}$ -like orbitals (for which the spin-splitting vanishes),  $\Xi_K^{so}$  stems from *interband* spin-orbit coupling between different  $d$  orbitals [21].

Having values of the spin-dependent scattering constants, we quantify the  $K$ -valley spin relaxation rate due to interaction with flexural phonons. For electrons, its contribution dominates all other processes in Table I. Using Fermi golden rule with (1) and assuming elastic scattering, the spin-flip rate of the  $\mathbf{k}$ -state is

$$\tau_s^{-1}(\mathbf{k}) \approx \frac{2m_{t(\ell)}(\Xi_K^{so})^2 k_B T}{\hbar^3 \varrho \gamma^2 (k'+k)^{2\eta-2}} \cdot {}_2F_1\left(\frac{1}{2}, \eta-1; 1; \frac{4kk'}{(k+k')^2}\right). \quad (3)$$

$\ell(t)$  denotes scattering from the top to lower spin-split bands (or vice-versa).  $m_{t(\ell)}$  is the effective mass and  $k' = \sqrt{m_{t(\ell)} k^2 / m_{\ell(t)} + (-)2m_{t(\ell)} \Delta_K / \hbar^2}$ . The hypergeometric function can be recast to simpler forms for case-specific  $\eta$  values. The respective expression for  $T$  valley spin flips is similar in form to (3), but with  $\eta \rightarrow \eta+1$  which reflects faster spin relaxation (as implied from Table I). We continue the analysis and calculate the  $K$ -valley spin relaxation rate in two limiting cases.

*free-standing monolayers.* Without a stiffening mechanism to suppress violent undulations, 2D membranes would crumple [34]. In crystal monolayers, such mechanism is naturally provided by the coupling between bending and stretching degrees of freedom. The coupling, in the lowest order that satisfies flat phase conditions, renormalizes the dispersion power law of long-wavelength flexural phonons from  $\eta=2$  to  $\eta=3/2$ , and it yields  $\gamma = \sqrt[4]{k_B T / \varrho v_0^2}$  where  $v_0 \approx v_{TA} \sqrt{1 - v_{TA}^2 / v_{LA}^2}$  is expressed in terms of the mode-dependent sound velocities [29, 34]. Using these parameters and assuming  $m_K \equiv m_t = m_{\ell}$ , the effective spin relaxation rate for Boltzmann distribution in the spin-split bands becomes

$$\frac{1}{\tau_s} = \sqrt{\frac{8\pi m_K}{\varrho v_0^2}} \left(\frac{\Xi_K^{so}}{\hbar}\right)^2 \left[ \frac{\text{Erfc}(\sqrt{\beta_K})}{1 + e^{-\beta_K}} \left(1 + \frac{0.1}{\sqrt{\beta_K}}\right) \right], \quad (4)$$

where  $\beta_K = \Delta_K / k_B T$ . Due to a relatively large valence-band splitting, the  $\beta_K > 1$  limit applies for holes at all practical cases where the temperature dependence is largely set by the complementary error function. Furthermore, in compounds with heavier transition-metal atoms (larger splitting), the flexural induced spin relaxation of holes is slower in spite of a larger  $\Xi_K^{so}$ . For example, in MoS<sub>2</sub> where  $\Delta_K^{(h)} = 160$  meV and in WS<sub>2</sub> where  $\Delta_K^{(h)} = 450$  meV [18], the flexural induced spin lifetimes at 300 K are, respectively,  $\sim 0.04$  ns and  $\sim 0.5$   $\mu$ s [35]. In addition to scattering with flexural phonons, the intrinsic spin relaxation of holes is affected by intravalley scattering with in-plane homopolar phonons [Fig. 2(b)], or by intervalley scattering between  $K$  and  $-K$ . Whereas the latter spin-flip scattering is forbidden in the zeroth-order by time reversal symmetry (Table I), it is not impeded by the relatively large spin splitting. Signatures of the homopolar and intervalley spin-flip mechanisms can be observed from their temperature dependence.

The spin relaxation of electrons is much faster due to the small spin splitting in the conduction band. In MoS<sub>2</sub>

where  $\Delta_K^{(e)} \approx 4$  meV [20], the room-temperature spin lifetime is  $\tau_s \sim 0.05$  ps [35], and it increases noticeably only below 50 K. Interestingly, the spin relaxation of electrons is enhanced in compounds with lighter metal atoms [their weaker spin-orbit coupling leads to smaller  $\Delta_K^{(e)}$ ]. Furthermore, the spin relaxation rate diverges in the pathological limit  $\Delta_K^{(e)} \rightarrow 0$  [37].

*supported monolayers.* Another means to stiffen the membrane is naturally provided by van der Waals (vdW) interactions when the monolayer is placed on a substrate [38]. The support brings in a minimum cutoff energy for out-of-plane displacements. The cutoff energy,  $\Omega_c = \hbar \sqrt{\kappa_s/M_u}$ , is calculated from the average vdW interatomic force constant between the monolayer and the substrate ( $\kappa_s$ ), and the average atomic mass of the monolayer ( $M_u$ ). In the long-wavelength limit, we can therefore approximate the dispersion of flexural phonons by  $\eta = 0$  and  $\gamma = \Omega_c/\hbar$ . The effective spin relaxation rate becomes

$$\frac{1}{\tau_s} = \frac{(2m_K \Xi_K^{so})^2}{\hbar^3 \rho} \cdot \frac{4 + 2\beta_K}{(1 + e^{\beta_K})\beta_c^2}, \quad (5)$$

where  $\beta_c = \Omega_c/k_B T < 1$  is assumed. The temperature dependence is quadratic for  $\beta_c < \beta_K < 1$  and exponential for  $\beta_c < 1 < \beta_K$ . The substrate coupling brings in slower relaxation that at room temperature reaches  $\tau_s \sim 3$  ps ( $\sim 0.2$  ns) for electrons (holes) in supported MoS<sub>2</sub> with  $\Omega_c \approx 1$  meV [39]. The spin-lifetime enhancement from  $\eta = 3/2$  to  $\eta = 0$  is sharper for electrons due to their smaller spin-splitting (phonons with longer wavelength are capable of inducing transitions between opposite spin bands). Figure 4 summarizes the temperature dependence of  $\tau_s$  for various SL-TMDs [35, 39].

We compare the spin relaxation induced by flexural phonons in graphene and MX<sub>2</sub>. The space inversion symmetry in graphene mandates spin-degenerate energy bands, resulting in anisotropic relaxation that depends on the spin orientation. Defining the latter by out-of-plane polar angle ( $\theta_s$ ) and in-plane azimuthal angle ( $\phi_s$ ), the spin-flip transition amplitude due to elastic scattering with flexural phonons follows (1) where

$$g(\mathbf{k}_i, \mathbf{k}_f) = ik \Xi_K^{so} \sin^2 \phi_- \left[ \sin^2 \frac{\theta_s}{2} e^{2i\phi_s - i\phi_+} + \cos^2 \frac{\theta_s}{2} e^{i\phi_+} \right]. \quad (6)$$

The other angles,  $\phi_{\pm} = \frac{1}{2}(\tan^{-1} \frac{k_{x,f}}{k_{y,f}} \pm \tan^{-1} \frac{k_{x,i}}{k_{y,i}})$ , are due to the Dirac-cone energy dispersion. Formal analytical derivation of this result will be presented in a future long publication. Here we mention that the prefactor  $k \sin^2 \phi_- = q^2/4k$ , previously found by numerical techniques [40], originates from space-inversion symmetry and spin-dependent energy dispersion in the cone region. Away from the Dirac point ( $k=0$ ), the spin relaxation timescales are longer in graphene than in SL-TMDs on accounts of the higher power-law in phonon wavevector ( $q^2$  vs  $q$ ) and the relative smallness of  $\Xi_K^{so}$  in carbon-based systems ( $\sim 10$  meV [41]).

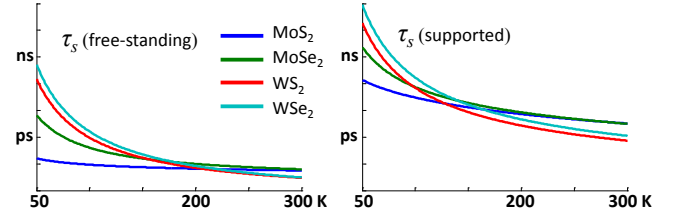


FIG. 4: (Color online) Electron spin lifetimes versus temperature, governed by intravalley scattering with flexural phonon for free-standing [Eq. (4)] and supported SL-TMDs [Eq. (5)].

All these findings lead to a counterintuitive relation between charge mobility and spin relaxation in 2D membranes. Whereas increased stiffness has been shown to be associated with slower spin relaxation, its coupling with charge mobility seems to have the opposite trend. For example, high mobility in supported membranes is a token of diminished effect from adsorbents and substrate imperfections. A smaller coupling of the membrane to such parasites would enable freer and softer out-of-plane undulations leading to ultrafast spin relaxation of electrons without affecting their mobility (forward spin-flip scattering by long-wavelength flexural phonons). Therefore, an inverse trend between spin and momentum relaxation, a hallmark of Dyakonov-Perel spin dephasing processes, can be realized in a Elliott-Yafet spin flip system. This physics is universal in relatively clean 2D membranes that respect mirror symmetry. In such membranes, charge transport is decoupled from harmonic out-of-plane undulations while spin relaxation is not severely affected by the presence of impurities.

In conclusion, we have presented a concise theory of intrinsic transport properties in single-layer transition-metal dichalcogenides. Lowest-order scattering processes were identified from group theory in both charge and spin transport regimes, and were found relevant to the transport of free-carriers at elevated temperatures and for the energy relaxation of hot excitons. In addition, the spin relaxation induced by scattering with long-wavelength flexural phonons was quantified. For electrons, the ultrafast rate is attributed to the typical softness of 2D membranes and to the small spin splitting in the conduction band. The relatively large splitting in the valence band, on the other hand, renders *p*-type monolayers better candidates for preserving spin information.

We are indebted to Professor Walter Lambrecht and Mr. Tawinan Cheiwchanchamnangij for insightful discussions and for sharing frozen-phonon DFT results prior to their publication. This work is supported by NRI-NSF, NSF, and DTRA Contract numbers DMR-1124601, ECCS-1231570, and HDTRA1-13-1-0013, respectively.

- 
- \* Electronic address: [yang.song@rochester.edu](mailto:yang.song@rochester.edu)
- [1] D. Xiao, G.-B. Liu, W. Feng, X. Xu, and W. Yao, *Phys. Rev. Lett.* **108**, 196802 (2012).
- [2] S. Cahangirov, C. Ataca, M. Topsakal, H. Sahin, and S. Ciraci, *Phys. Rev. Lett.* **108**, 126103 (2012).
- [3] H.-Z. Lu, W. Yao, D. Xiao, and S.-Q. Shen, *Phys. Rev. Lett.* **110**, 016806 (2013).
- [4] K. F. Mak, C. Lee, J. Hone, J. Shan, and T. F. Heinz, *Phys. Rev. Lett.* **105**, 136805 (2010).
- [5] A. Splendiani, L. Sun, Y. Zhang, T. Li, J. Kim, C.-Y. Chim, G. Galli, and F. Wang, *Nano Lett.* **10**, 1271 (2010).
- [6] T. Korn, S. Heydrich, M. Hirmer, J. Schmutzler, and C. Schüller, *Appl. Phys. Lett.* **99**, 102109 (2011).
- [7] T. Cao, G. Wang, W. Han, H. Ye, C. Zhu, J. Shi, Q. Niu, P. Tan, E. Wang *et al.*, *Nat. Comm.* **3**, 887 (2012).
- [8] B. Radisavljevic, A. Radenovic, J. Brivio, V. Giacometti, and A. Kis, *Nat. Nano.* **6**, 147 (2011).
- [9] S. Kim, A. Konar, W.-S. Hwang, J. H. Lee, J. Lee, J. Yang, C. Jung, H. Kim, J.-B. Yoo *et al.*, *Nat. Comm.* **3**, 1011 (2012).
- [10] K. Kaasbjerg, K. S. Thygesen, and K. W. Jacobsen, *Phys. Rev. B.* **85**, 115317 (2012).
- [11] H. Zeng, J. Dai, W. Yao, D. Xiao, and X. Cui, *Nat. Nano.* **7**, 490 (2012).
- [12] K. F. Mak, K. L. He, J. Shan and T. F. Heinz, *Nat. Nano.* **7**, 494 (2012).
- [13] G. Sallen, L. Bouet, X. Marie, G. Wang, C. R. Zhu, W. P. Han, Y. Lu, P. H. Tan, T. Amand *et al.*, *Phys. Rev. B* **86**, 081301(R) (2012).
- [14] G. Kioseoglou, A. T. Hanbicki, M. Currie, A. L. Friedman, D. Gunlycke, and B. T. Jonker, *Appl. Phys. Lett.* **101**, 221907 (2012).
- [15] R. Fivaz and E. Mooser, *Phys. Rev.* **163**, 743 (1967).
- [16] A. Wilson and A. D. Yoffe, *Adv. Phys.* **18**, 193 (1969).
- [17] L. F. Mattheiss, *Phys. Rev. B.* **8**, 3719 (1973).
- [18] Z. Y. Zhu, Y. C. Cheng, and U. Schwingenschlögl, *Phys. Rev. B* **84**, 153402 (2011).
- [19] A. Molina-Sánchez and L. Wirtz, *Phys. Rev. B.* **84**, 155413 (2011).
- [20] T. Cheiwchanamangij and W. R. L. Lambrecht, *Phys. Rev. B* **85**, 205302 (2012).
- [21] See supplemental material for character tables, association of states with irreducible representations, integrals of scattering constants, and optical properties of excitons.
- [22] Y. Song and H. Dery, *Phys. Rev. B* **86**, 085201 (2012).
- [23] J. Gunn, *IBM J. Res. Dev.* **8**, 141 (1964).
- [24] H. Kroemer, *Proc. IEEE* **52**, 1736 (1964).
- [25] J. Li, L. Qing, H. Dery, and I. Appelbaum, *Phys. Rev. Lett.* **108**, 157201 (2012).
- [26] The reduced screening in 2D renders a relatively large exciton binding energy such that  $E_{A,B}$  in Fig. 3 lie well below the one-particle energy gaps [12, 20].
- [27] R. J. Elliott, *Phys. Rev.* **108**, 1384 (1957).
- [28] In addition, spin flops due to electron-hole exchange (Bir-Aronov-Pikus mechanism) are typically too slow to account for the measured reduction in the circular polarization degree (see supplemental material in [12]).
- [29] E. Mariani and F. von Oppen, *Phys. Rev. Lett.* **100**, 076801 (2008).
- [30] Y. Yafet, *Solid State Physics*, edited by F. Seitz and D. Turnbull (Academic, New York, 1963), Vol. 14, p. 1.
- [31] Symmetry based analysis of the respective spin-conserving scattering is provided in the supplemental material.
- [32] G. L. Bir and G. E. Pikus, *Symmetry and Strain-induced Effects in Semiconductors* (Halsted Press, Jerusalem, 1974), Chapters 3-4.
- [33] Independently, Tawinan Cheiwchanamangij and Walter Lambrecht got similar results by using a full-potential linearized muffin-tin orbital method (unpublished).
- [34] D. R. Nelson and L. Peliti, *J. Phys. (Paris)* **48**, 1085 (1987).
- [35] The crystal mass density and sound velocities of MoS<sub>2</sub>, MoSe<sub>2</sub>, WS<sub>2</sub> and WSe<sub>2</sub> are  $\rho \approx 3.1, 4.9, 4.8, 6.6 \times 10^{-7}$  gr/cm<sup>2</sup>,  $v_{TA(LA)} \approx 4.2(6.7), 3.5(4.9), 4.0(6.5), 3.6(4.6) \times 10^5$  cm/s, respectively [10, 20, 36]. Using ABINIT DFT code, the respective values of  $\Delta^e_K \approx$  are 4, 22, 41, 47 meV. In addition, for all compounds  $m_K \sim 0.5m_0$ .
- [36] C. Ataca, H. Şahin, and S. Ciraci, *J. Phys. Chem. C* **116**, 8983 (2012)
- [37] By repeating the analysis for suspended monolayers for which  $\eta = 1$  and  $\gamma = v_0\sqrt{\epsilon}$ , we find that  $\tau_s < 1$  ps at 300 K even for suspension-induced strain levels of  $\bar{\epsilon} \sim 1\%$ .
- [38] J.-H. Seol, I. Jo, A. L. Moore, L. Lindsay, Z. H. Aitken, M. T. Pettes, X. Li, Z. Yao, R. Huang *et al.*, *Science* **328**, 213 (2010).
- [39] We assumed a force constant of  $\sim 0.4$  N/m, similar to the one found in graphene on SiO<sub>2</sub> [38]. We use similar cutoff energy  $\Omega_c \approx 1$  meV for other compounds in Fig. 4.
- [40] S. Fratini, D. Gosálbez-Martnez, P. Merodio Cámara, J. Fernández-Rossier, arXiv:1202.6216 (2012).
- [41] D. Huertas-Hernando, F. Guinea, and A. Brataas, *Phys. Rev. B* **74**, 155426 (2006).